JOURNAL OF GEOPHYSICAL RESEARCH, VOL. 103, NO. C5, PAGES 10,469–10,487, MAY 15, 1998

Application of the adjoint of the WAM model to inverse wave modeling

H. Hersbach

Royal Netherlands Meteorological Institute, De Bilt

Abstract. In this paper the adjoint to the full WAM model, a third-generation ocean wave model, is presented. This adjoint, ADWAM, was constructed from the WAM source code level by using an automatic adjoint code generator. As a first application, ADWAM has been used for inverse modeling with the object to get a better insight into the numerical values of several model parameters in the WAM source terms. Two adjoint runs were performed. For the first, both deep water fetch data, which were compiled by Kahma and Calkoen, and shallow water fetch data, which were obtained from Lake George by Young and Verhagen, were considered simultaneously. The second adjoint run was performed for a storm which occurred in the North Sea in February 1993. Both adjoint runs lead to a consistent trend: a reduction in the integral strengths of both the wind input and the whitecapping source terms with respect to the best estimate so far. In this best estimate, the whitecapping dissipation is proportional to the square of the wave steepness. Both runs in addition suggested that this dependency should be increased to a cubic one. It was found that the improved model performance was not only limited to the optimization windows but consistent for other intervals that were not optimized.

1. Introduction

Modern (third-generation) ocean wave prediction [see, e.g., *Komen et al.*, 1994] is based on numerical integration of the energy balance equation, which is the basic equation describing the generation, interaction, propagation and decay of ocean waves. Each of these terms describes a physical process. For example, the wind input term represents the transfer of momentum from the atmospheric boundary layer to the waves. Ideally, perfect knowledge of these microphysical processes would lead to a perfect wave prediction model and to accurate wave prediction. However, reality is not perfect. The values of some model constants are only known to a limited accuracy. In fact, their values may even vary in space and time because they depend on other unresolved parameters. The dissipation constant is an example of a constant that has not been measured directly nor has it been determined from first principles. *Komen et al.* [1994] fixed this constant by requiring that integrated wave evolution reaches a steady state in agreement with observations by *Pierson and Moskowitz* [1964]. In essence, the constant was determined from observations of the integrated wave evolution and from source term balance. Wind input constants are known better, both from theory and from direct measurements, but the error in the estimate, at least 20 %, still leaves some freedom. In addition, the actual value in a given situation may depend on the gustiness, or on the presence of slicks or even on biological activity. Bottom dissipation depends on details of the bottom structure, which are often not known. The bottom dissipation constant may vary in space in the case of an inhomogeneous bottom structure, or even vary in time when bottom ripples are being generated. On a sandy bottom all of these uncertainties contribute to the error in wave prediction.

Another important source of error comes from errors in the forcing. In fact, *Cardone et al.* [1995] discuss a situation in which the errors in wind fields produced at operational centers contribute much more to the error in the wave forecast than the systematic errors in the underlying wave physics.

It is very difficult to get a better idea about the precise form and strength of the above mentioned source terms from first principles. Therefore, as an alternative, one can try to get a better picture of the source terms by comparing model results to observations, using a data assimilation scheme.

Data assimilation can be done in a number of ways. Usually, a cost function (expressing the misfit between model results and the available data within the considered period) is to be minimized with respect to a set of control variables. The choice of the control variables depends on the application. If one is interested in the best initial field or driving field, these are taken as the

Paper number 97JC03554.
0148-0227/98/97JC-03554$09.00

control variables. When model performance is to be improved, which is referred to as inverse modeling, the control variables represent model parameters.

An efficient minimization of the cost function requires gradient information with respect to the control variables. The calculation of these gradients is in general quite complex. Therefore, as an alternative, one can approximate the gradient on the basis of finite differences. This has for the fine tuning of the WAM physics been done by *Monbaliu* [1992a, b], in which a stationary, one-dimensional version of WAM applicable to fetch-limited growth relations was considered. The drawback of the finite difference method is that each component of the gradient requires one extra model run. For this reason, Monbaliu was able to allow for the variation of only two control variables at a time. For a realistic situation, that is, the implementation of the full-dimensional WAM model on, for example, the North Sea, the finite difference method becomes too expensive. Usually, the number of control variables for inverse modeling is not so large, but if one would like to adjust a whole field, such as a driving wind field, or details of the bathymetry, the finite difference method is far beyond computational limits.

The complexity of the calculation of the gradient can be disentangled by the so-called adjoint model. This adjoint model, which is to be derived from the model that calculates the cost, is able to trace back all dependencies in a very efficient way. Therefore the adjoint model is able to combine not only information at one time step (which is the case for sequential methods such as optimal interpolation), but for the whole assimilation run. The dependencies are traced in the reverse order in which the cost was calculated. Therefore one speaks about the forward model and its backward adjoint model.

The evaluation of any gradient requires one adjoint run only. The computational burden, usually of the order of two forward model runs, is therefore independent of the number of control variables. This makes the adjoint method very suitable when the number of control variables is large. The adjoint of the one-grid point version of the WAM model has been successfully applied to assimilate the initial wave field by *De las Heras and Janssen* [1992] and *De las Heras et al.* [1994]. *De Valk and Calkoen* [1989] have assimilated forcing wind fields into a third-generation wave model on the basis of the adjoint to their second-generation model. An alternative approach in order to correct the forcing wind field was presented by *Bauer et al.* [1996]. Rather than using the adjoint, an approximation to the Green's function describing the linear response of the wave field with respect to a change in the wind field was successfully applied. An inverse modeling application was given by Barzel and Long [*Barzel,* 1994; *Komen et al.,* 1994], who have considered a similar case as Monbaliu, that is, fetch limited growth. Their results are based on the adjoint of the one-dimensional stationary WAM model. Their adjoint approach allowed for more independent control variables in the source terms than the finite difference approach of Monbaliu. However, they found that the wave information contained in the fetch-limited case (wind sea only), was not sufficient to resolve the details of the individual source terms. Therefore *Barzel* [1994] recommended to test the WAM physics in a more complex, realistic environment, using the adjoint of the full model. This has been done in the research described in this paper.

A technical complication of the adjoint method is that one first has to derive the adjoint model from the forward model equations. This can be a very tedious operation. In the case of the WAM model, for instance, the derivation of the adjoint to the nonlinear interactions is very complex [*De las Heras et al.,* 1994]. This is the reason why in the work quoted above, restrictions were made in the dimensionality or complexity of the underlying wave model.

As an alternative, one can also derive adjoint code on the computer code level. In this case one regards the computer source code that represents the numerical implementation of the model as the forward model. The adjoining of this can be performed line by line, using rather simple and straightforward rules. Recently, Giering of Max-Planck-Institut Hamburg has developed an adjoint model compiler (AMC [see *Giering and Kaminski* 1997]), which is able to adjoin computer code automatically. As input, AMC requires the Fortran 77 source code; as output, it returns the source code of the adjoint model.

Using this compiler it was possible to generate the adjoint of the full-dimensional WAM model (i.e., two-dimensional (2-D) in physical space, 2-D in spectral space, plus time). The resulting adjoint code, ADWAM, can be used in realistic situations for the assimilation of wind fields, initial fields, and model parameters. No restrictions in the dimensionality or complexity of the wave model had to be made.

Two different adjoint runs have been performed. The first application, which is described in section 2, considers fetch-limited growth. This situation is ideal to test wind sea generation in the model. Both the deep water case and the shallow water case were optimized simultaneously. For the deep water case, WAM results obtained from an idealized deep ocean with an off-land wind were compared to the fetch laws for significant wave heights and peak frequencies compiled by *Kahma and Calkoen* [1992]. These fetch laws represent the average of a number of extensive measurements campaigns. This therefore represents a somewhat artificial situation. The shallow water case, however, reflects a realistic situation. Fetch-limited wave heights and peak frequencies were obtained from Lake George (a shallow lake near Canberra, Australia) by *Young and Verhagen* [1996]. WAM model results of the implementation on Lake George were compared to these data.

As a second application, the so-called Wadden storm of February 1993, was considered. This storm in the North Sea represents an extreme situation in wave conditions. In addition, the North Sea is a region in which both deep and shallow water and both wind sea and swell are important. This storm in the North Sea region was also selected as the test case in the European Coupled Atmosphere Wave Ocean Model (ECAWOM) project, which aims at the construction of a coupled atmospheric-wave-ocean model including a data assimilation environment. The work presented in this paper is part of this project. This application is described in section 3. In section 4, conclusions and recommendations are formulated. Appendix A gives a concise description of the WAM physics. A comprehensive description is given by *Komen et al.* [1994]. In Appendix B a brief description of how ADWAM was generated is presented. A more detailed description of this adjoining operation is given by *Hersbach* [1997].

2. Fetch-Limited Growth

The experimentally well-explored situation of fetch-limited growth was chosen as a first application. In this situation an off-land wind blows from a (in the ideal case infinitely long) coastline. When the duration of this wind is long enough, a time-independent, but fetch- (the up-wind distance from the coast line) dependent situation will occur. Wave heights increase and peak frequencies decrease with increasing fetch.

In one single adjoint run, both the deep water case and the shallow water case were optimized simultaneously. For the deep water case, model results were compared to growth curves established by *Kahma and Calkoen* [1992]. These curves for wave energy and peak frequency are based on a large number of observations collected by various extensive measurement campaigns. For the shallow water case, the model output was compared to the data obtained by *Young and Verhagen* [1996]. To this end the WAM model was implemented for Lake George, the location at which the measurements were performed.

2.1. Deep Water Data

For the deep water fetch-limited case, *Kahma and Calkoen* [1992] reanalyzed the data of a number of experiments. As a result, they established relations for wave energy E and peak frequency f_p as a function of fetch X. In the evaluation of these so-called growth curves or growth laws, Kahma and Calkoen discriminated between stable and unstable stratification. In addition, they also produced growth laws on the basis of the composite data set, that is, where no distinction for stratification was made. Because WAM does not take any form of stratification into account, we will compare our model results with these latter growth curves.

Growth curves are based on scaling laws with respect to the driving wind fields. We believe that the friction velocity u_* is the correct scaling parameter. However, usually only U_{10}, that is, the wind speed at 10 m is available. Therefore when composing growth curves, u_* has first to be deduced from U_{10}. The relation between these two velocities is determined via the roughness length z_0 of the wave surface:

$$C_D \equiv \left(\frac{u_*}{u(z)}\right)^2 = \frac{\kappa^2}{\ln^2(z/z_0)}, \tag{1}$$

in which C_D is the drag coefficient and z=10 m.

In principle, z_0 depends on the sea state. The determination of the strength and details of this dependency is very delicate. A great deal of research in this direction has been carried out and is still going on. In WAM, z_0 depends in a detailed way on the wave spectrum [*Janssen,* 1989, 1991]. In other formulations, the wave-state dependency only enters via the wave age (u_*/c) [see, e.g., *Smith et al.,* 1992; *Donelan,* 1990]. *Kahma and Calkoen* [1992] also established growth curves that take a wave-state dependency on the roughness length into account, by assuming a wave-age dependent drag coefficient proposed by *Donelan* [1990] (see 5)). These are the growth laws against which the WAM results were verified.

Given the experimental fetch ranges that were available, the growth curves of Kahma and Calkoen are only valid for the moderate fetch range. However, it is known that for a fully developed sea, that is, infinite fetch, wave energy and peak frequency will saturate to the *Pierson-Moskowitz* [1964] values.

Combining the results of Kahma and Calkoen with those of Pierson and Moskowitz, we obtained the following growth curves:

$$\epsilon^* = 1.1 \times 10^3 (1 + 9.51 \times 10^6 / X^*)^{-0.96}, \tag{2}$$

$$f_p^* = 5.6 \times 10^{-3} (1 + 1.45 \times 10^7 / X^*)^{0.29}. \tag{3}$$

The dimensionless energy ϵ^*, peak frequency f_p^* and fetch X^* are related to their observed quantities E^{KC}, f_p^{KC} and X by (the superscript KC stands for data considered by Kahma and Calkoen):

$$E^{\mathrm{KC}} = \epsilon^* \frac{u_*^4}{g^2}, \quad f_p^{\mathrm{KC}} = f_p^* \frac{g}{u_*}, \quad X = X^* \frac{u_*^2}{g}, \tag{4}$$

where the friction velocity u_* was calculated from U_{10}^{KC} and the "wave state" $(E^{\mathrm{KC}}, f_p^{\mathrm{KC}})$ using the wave state dependent z_0 relation proposed by *Donelan* [1990] (κ = 0.41 is von Kármán's constant):

$$\begin{aligned} U_{10}^{\mathrm{KC}} &= \frac{u_*}{\kappa} \ln(10/z_0), \\ z_0 &= 5.53 \times 10^{-4} \frac{2\pi f_p^{\mathrm{KC}}}{g} U_{10}^{\mathrm{KC}} \sqrt{E^{\mathrm{KC}}}. \end{aligned} \tag{5}$$

2.2. Shallow Water Data

For the shallow water fetch-limited case, *Young and Verhagen* [1996] performed an extensive experiment in Lake George (35.2°S, 149°E), near Canberra, Australia.

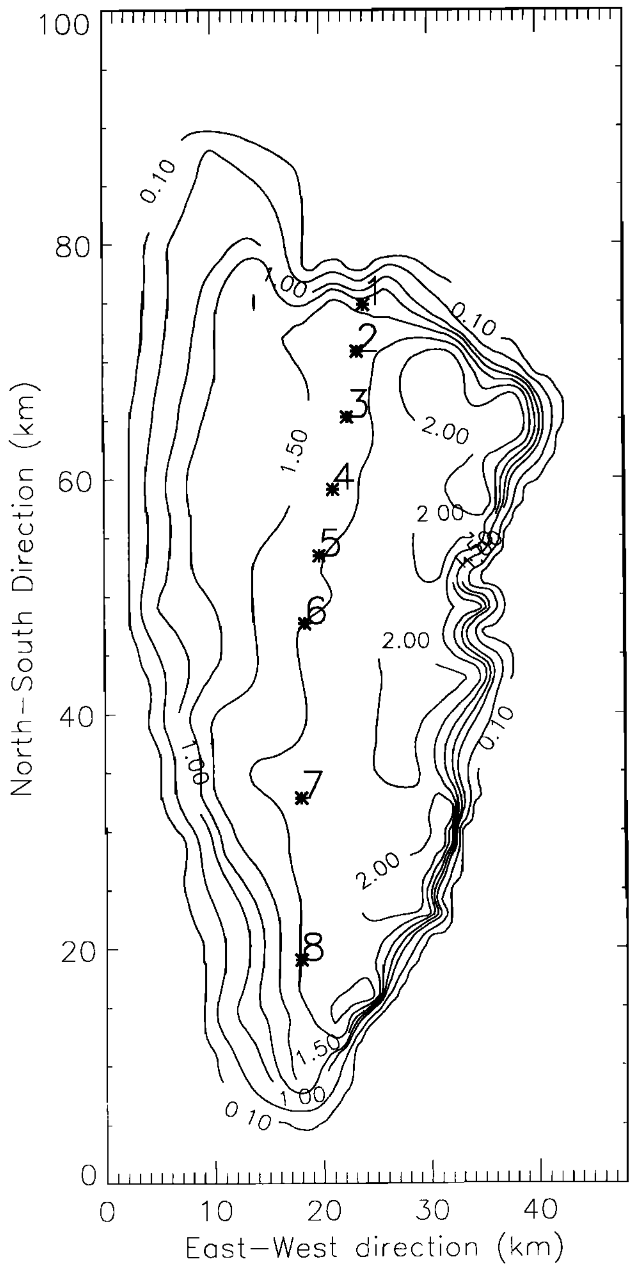

Figure 1. Bathymetry for Lake George. The depths are in meters. The numbers 1-8 indicate the location of the corresponding stations.

A detailed description of the experimental setup is given by *Young and Verhagen* [1996]. Here we will only present a brief summary. Lake George is approximately 20 km long and 10 km wide and has a flat bottom of about 2 m depth. A series of eight measurement stations were established along the N-S axis as shown in Figure 1. At station 6 (which is located in the middle of the lake) the U_{10} wind speed was measured. From this wind speed the winds at all locations were reconstructed, by assuming an internal boundary layer, which describes the land-lake transition. For this the relation given by *Taylor and Lee* [1984] was used, which depends on the ratio between the surface roughnesses of the lake (z_0) and of the up-wind land z. In principle, for z_0 the WAM formulation of the wave state dependent roughness length should be used. So in principle, the determination of the internal boundary layer for the wind field and the calculation of the wave field are coupled. However, the coupling is very weak. Therefore for the determination of the internal boundary layer, z_0 was assumed to be uniform over the lake and was derived from U_{10} at station 6 by using a fixed *Charnock* [1955] relation: $z_0 = 0.0185\,(u_*^2/g)$. The difference in resulting wind fields when using the wave state dependent roughness is negligible. According to *Young and Verhagen* [1996], for the roughness at land, z=0.1 m for northerly and westerly winds, and z=0.5 m for southerly and easterly winds give results that are compatible with the occasional wind measurements at all stations.

At each station (if operational), wave data were obtained on an hourly basis using Zwarts poles (for a description, see *Young and Verhagen* [1996]). For the present application the following are relevant:

$\mathbf{U}_{10}$	10 m wind vector (m/s), only at station 6;
H_s^{LG}	significant wave height (m);
$H_{\min}^{\mathrm{LG}}, H_{\max}^{\mathrm{LG}}$	confidence levels of H_s^{LG} (m);
f_p^{LG}	peak frequency (Hz);
d^{LG}	local water depth (m).

2.3. WAM Setup

The available 250 × 250 m Lake George bathymetry file was rotated and scaled, such that most poles are close to grid points. A counterclockwise rotation of 13° and a grid spacing of 1/80 degree = 1.39 km, gave satisfactory results. On this grid, WAM was inplemented. An integration time step of 180 s and a frequency domain from FR(1) = 0.2 Hz - FR(25) = 2.0 Hz was found to be suitable and compatible with the Courant-Friedrichs-Levy (CFL) criterion. At the east end of the Lake George grid one extra north-south line of 15 "sea" points with infinite depth was added. Each point of this line was chosen to be its own east-west neighbor. Therefore in combination with a southern constant wind this exactly mimics the situation of an infinite coastline. The total number of sea plus lake points was 90.

As a test, runs on the basis of a finer grid and higher time resolution were performed. Only a negligible difference in results (< 1 cm in H_s) was obtained, which gave confidence on the reliability of the discretization.

Using this setup, both the deep water fetch case (the N-S line) and the shallow water fetch case (the Lake George bathymetry) could be optimized simultaneously. So part of the grid represents a true deep water case, the remaining part represents a true shallow water case.

The Lake George part of the grid was forced with the observed wind fields (see the previous subsection), the fetch line was forced with a constant southerly wind of $U_{10} = 10\,\mathrm{m/s}$ ($u_* \sim 0.38\,\mathrm{m/s}$). Using (4) it is found that the deep water line corresponds to $X^* \in [1 \times 10^5, 1.5 \times 10^6]$, which is well situated in the fetch range considered by *Kahma and Calkoen* [1992].

2.4. Choice of the Control Variables

The data obtained from this first assimilation experiment only concern integrated parameters, that is, give only limited information about the two-dimensional structure of the wave spectra. In addition, the wave spectra only contain wind sea. Therefore we chose to use a limited number of model parameters as control variables.

A main interest is the relative strength between the wind input and whitecap dissipation. Therefore their overall strengths were allowed to vary.

In WAM the significant wave height and peak frequency are closely connected: an increase of wave height will in general be accompanied with a decrease of peak frequency. This relation can be expressed by the dimensionless quantity:

$$Y_p = H_s f_p^2 / g. \tag{6}$$

Because of its dimensionless nature, Y_p can only depend on dimensionless quantities. In the case of fetch-limited growth, the only relevant dimensionless quantity is the dimensionless wave age c_p/u_*, or equivalently, the dimensionless fetch X^* (see (4)). From (2)-(4) in combination with $H_s = 4\sqrt{E}$ it follows that Y_p depends only mildly on wave age:

$$Y_p \approx 4.2 \times 10^{-3} \ \max\left\{1.0, \left(\frac{1.2 \times 10^8}{X^*}\right)^{0.1}\right\}. \tag{7}$$

Therefore the value of Y_p will be quite insensitive to external quantities, such as a driving wind field or fetch. It will be mainly a result of the model physics, especially the balance between S_{in} and S_{dis}. For a wind-sea spectrum the peak frequency is proportional to the square root of a typical wave number $< k >$ (the relation between these two quantities is given by the dispersion relation). Therefore the parameter Y_p is related to the steepness $\sqrt{\alpha}$ (defined by (A6)) of the spectrum. From this consideration it is expected that Y_p will be sensitive to the power D_s to which α is raised in the whitecap dissipation (A5). In order to investigate this conjecture, D_s was taken as one of the control variables.

As was stated in section 2.4, the strength C_{bot} of the bottom dissipation may depend very much on the sediment, which for Lake George consists of a "relative fine grained but cohesive mud. The bed is not mobile and ripples do not appear" [*Young and Verhagen*, 1996, page 76]. To investigate whether this sediment should give rise to a strength of bottom dissipation different from the Joint North Sea Wave Project (JONSWAP) strength, C_{bot} was also allowed to vary.

Due to seasonal influences, the water depth of Lake George is not constant in time. In order to be able to correct the available bathymetry file for this, the local WAM depth d^{WAM} at each grid point was also allowed to be adjusted. In principle one parameter could take account of the integral offset of the water depth of the whole lake. However, to allow more freedom, such as a tilt, the water depth was allowed to be adjusted independently at each grid point. In order to avoid that a minimization run will only result in a modification of the water depth at the locations of the poles, the square of a Laplacian term $\Delta d = (\partial^2/\partial x^2 + \partial^2/\partial y^2) d(x,y)$ was added to the cost. Such a term inhibits localized modifications because it is proportional to the curvature of the correction field. Only an overall offset and an overall tilt of the bathymetry (for which $\Delta d = 0$) will give zero contributions. Therefore this first-guess penalty effectively distributes the localized depth information over all grid points.

To summarize, the following control variables were chosen:

$$\begin{aligned} \beta_m &\rightarrow C_1 \beta_m \\ C_{\mathrm{dis}} &\rightarrow C_2 C_{\mathrm{dis}} \\ D_s &\rightarrow C_3 D_s \\ C_{\mathrm{bot}} &\rightarrow C_4 C_{\mathrm{bot}} \\ d^{\mathrm{WAM}}_{(x,y)} &\rightarrow d^{\mathrm{WAM}}_{(x,y)} + d_0 * C_{(x,y)}, \quad d_0 = 0.1\mathrm{m}. \end{aligned} \tag{8}$$

The total number of control variables is 4 + 90 = 94.

2.5. Cost Function

The cost function J used consists of three parts:

$$J(\vec{C}) = J_{\mathrm{LG}}(\vec{C}) + J_{\mathrm{KC}}(\vec{C}) + J_{\mathrm{FG}}(\vec{C}). \tag{9}$$

The first part, J_{LG}, reflects the misfit of the model results with the Lake George data. It contains a comparison between the observed and modeled wave heights and peak frequencies. In addition, the water depths used in the WAM run are compared to the observed water depths. The precise form of J_{LG} is

$$J_{\mathrm{LG}} = \sum_{i=\mathrm{time,\,stations}} \left\{ w_i \left(\frac{H_i^{\mathrm{WAM}} - H_i^{\mathrm{LG}}}{H_i^{\mathrm{LG}}}\right)^2 + w_i \left(\frac{f_{p,i}^{\mathrm{WAM}} - f_{p,i}^{\mathrm{LG}}}{f_{p,i}^{\mathrm{LG}}}\right)^2 + w_d \left(\frac{d_i^{\mathrm{WAM}} - d_i^{\mathrm{LG}}}{d_i^{\mathrm{LG}}}\right)^2 \right\}. \tag{10}$$

The sum contains the contribution for each measurement at each station during the whole assimilation period.

This contribution to the total cost contains the dimensionless weights w_i and w_d. The weights for the wave heights can be deduced from the observed confidence levels $H_{\min}^{\mathrm{LG}}$ and $H_{\max}^{\mathrm{LG}}$. For the peak frequency, however, such confidence levels are not available. Therefore the relative weights for f_p were chosen to be equal to those of H_s:

$$w_i = \left(\frac{H_i^{\mathrm{LG}}}{(H_{\max}^{\mathrm{LG}})_i - (H_{\min}^{\mathrm{LG}})_i} \right)^2 . \quad (11)$$

Also no confidence levels for the measured depths were available. We chose to weight the misfit in depth in a mild way. Therefore the small value of

$$w_d = 0.4 \quad (12)$$

was taken.

The second term in the cost function (J_{KC}) reflects the model performance for the deep water part:

$$J_{\mathrm{KC}} = w_{\mathrm{KC}} \sum_{i=\text{fetchline}} \left\{ 2 \left(\frac{E_i^{\mathrm{WAM}} - E_i^{\mathrm{KC}}}{E_i^{\mathrm{KC}}} \right)^2 + \left(\frac{f_{p,i}^{\mathrm{WAM}} - f_{p,i}^{\mathrm{KC}}}{f_{p,i}^{\mathrm{KC}}} \right)^2 \right\} . \quad (13)$$

To ensure that the modeled spectra are fully developed in time, only a comparison with the Kahma-Calkoen fetch lines is made at the end date of the assimilation run. The accuracy of the Kahma-Calkoen fits is not well known. Therefore the correct value (i.e., from a statistical point of view) of w_{KC} cannot be given. If one assumes that typically $f_{\max}^{\mathrm{KC}} - f_{\min}^{\mathrm{KC}} \approx 0.1 f^{\mathrm{KC}}$, one would expect $w_{\mathrm{KC}} \sim 100$. However, to compensate for the fact that there are fewer "data" points for the deep water line than for Lake George, it was decided to double this value:

$$w_{\mathrm{KC}} = 200.$$

The third term in the total cost represents a penalty for a too large deviation from the first guess fields. First of all, in order to express confidence in previous research, it is undesirable for the power D_s in the whitecap dissipation term to deviate too much from its default value. For the same reason, such penalty terms would also be desirable for a combination of the strengths of S_{in} and S_{dis}. However, the comparison to the deep water growth curves effectively already takes care of this. The strength of the bottom dissipation depends very much on the sediment. Therefore no first-guess penalty for this parameter was included.

The depth at each grid point was allowed to be adapted independently. The penalty for a misfit in water depth in J_{LG} concerns only the locations of the stations. As was discussed in the previous subsection, the knowledge of the water depths at the stations was distributed to other grid points by adding a Laplacian penalty $J \sim (\Delta d^{\mathrm{WAM}})^2$.

As a result, the following first-guess penalty was used:

$$J_{\mathrm{FG}} = 400(D_s - 2)^2 + w_d \sum_{(x,y)\in\text{grid}} (\Delta d^{\mathrm{WAM}})^2_{x,y} \quad (14)$$

where

$$(\Delta d)_{x,y} = \frac{4d_{x,y} - d_{x,y+1} - d_{x,y-1} - d_{x+1,y} - d_{x-1,y}}{d_{x,y}} .$$

For the weight w_d the same value as in J_{LG} was used.

2.6. Optimization

From the huge Lake George data set (67,225 data points), the 12-hour period June 9, 1993, 0000-1200 UT was selected for performing the adjoint optimization. For this period the wind was northerly and had a strength of $U_{10} \sim 5$ - 8 m/s.

The cost function (9) was minimized with respect to the control variables (8). For this, the minimiza-

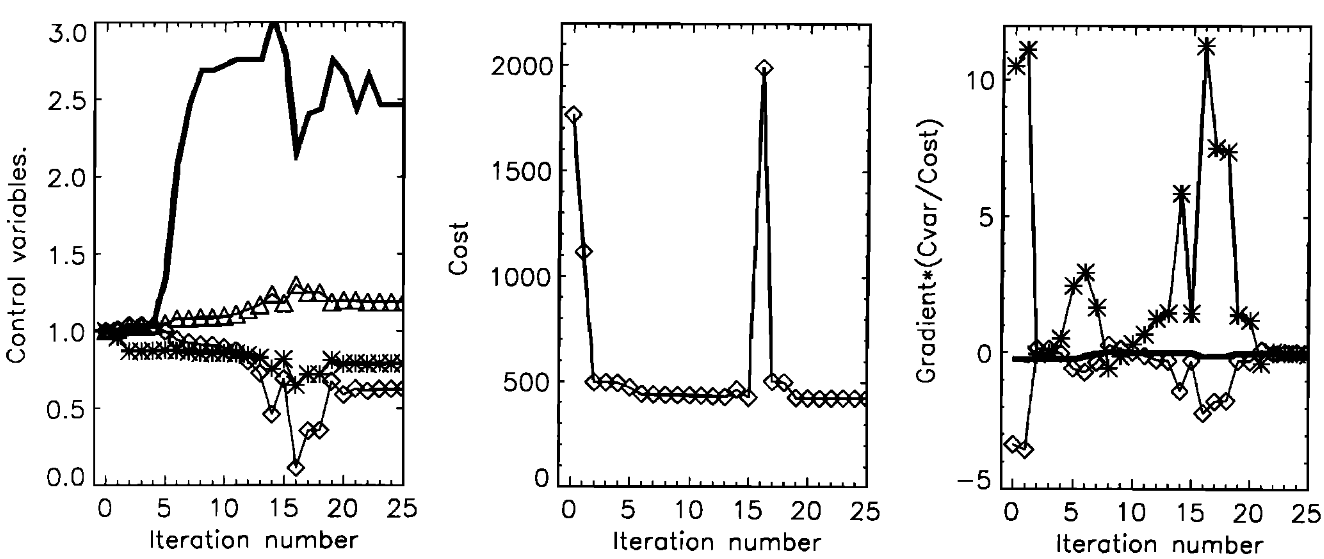

Figure 2. Optimization for the fetch-limited case. (left) Evolution of the control parameters β_m (asterisks), C_{dis} (diamonds), D_s (triangles), and C_{bot} (solid line). (middle) Evolution of the cost. (right) Evolution of relative gradients for control variables β_m (asterisks), C_{dis} (diamonds), and C_{bot} (solid line). The relative gradient for D_s is very similar to the relative gradient for C_{dis}.

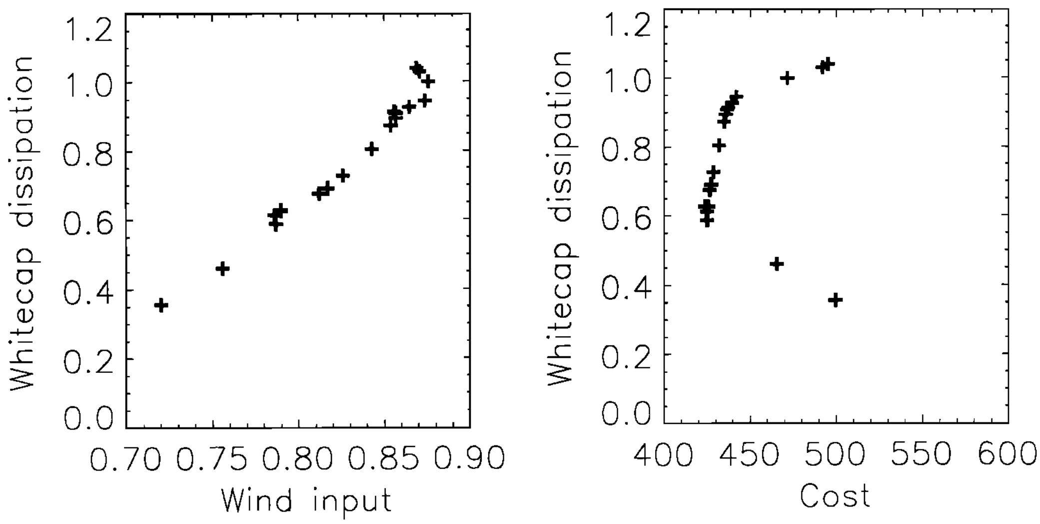

Figure 3. Scatterplot of (left) the strength of the whitecapping versus the strength of the wind input and (right) whitecapping versus the value of the cost. Only points explored by the adjoint optimization that gave rise to a cost lower than 500 are displayed.

tion package MODULOPT developed at Institut National de Recherche en Informatique et en Automatique, France, was used. This routine is based on the quasi-Newton method. A comprehensive description is given by *Gilbert and Lemaréchal* [1989]. The gradient required by the minimizing routine was calculated with the adjoint model. The resulting fit is presented in Figure 2. Numerical values are given in Table 1. It is seen that there is a fast convergence (within two steps) to a minimum. At this local minimum the only significant change is a reduction of the strength of the wind input term. As can be seen from Table 1, at this minimum, especially J_{KC} has been reduced enormously. Apparently, it is not difficult to find a parameter set that obeys deep water fetch relations. At the fifth iteration, a transition to a new local minimum occurs. In this transition the strength of the bottom dissipation is more than doubled. The decrease of the cost is much smaller. However, it is only J_{LG} that is improved now. Apparently, it is more difficult to find a parameter set that in addition

Table 1. Numerical Values of the Control Variables, Defined by (8), Before Optimization (Default), at Iteration 4 and After Optimization (Final Fit)

Quantity	C_{var}	Default	Iteration 4	Final Fit
Strength S_{in}	C_1	1.0	0.78	0.79
Strength S_{dis}	C_2	1.0	1.03	0.63
Steepness S_{dis}	C_3	1.0	1.04	1.20
Strength S_{bot}	C_4	1.0	1.02	2.43
Offset depth	$C_{(x,y)}$	0.0	$\sim$ 0.0	$\sim$ 0.0
First guess	J_{FG}	0	6	21
Kahma-Calkoen	J_{KC}	1140	90	87
Lake George	J_{LG}	624	396	316
Total cost	J	1764	492	424

to deep water leads to best results for shallow water. Finally, around the 15th iteration a second transition occurs. This relaxes to a third local minimum. From the 25th up to the 40th iteration (the last iteration performed, not displayed in Figure 2) the system remains in this minimum.

From the fact that several quite different locations in control space give rise to very similar local minima, it may be concluded that the cost function contains a valley. Apparently, the fetch-limited growth situation is not able to completely restrict the strength of each source. This can be most clearly seen from Figure 3. The left panel of Figure 3 shows a scatterplot of the strength of the wind input versus the strength of the whitecap dissipation, for all points explored during the minimization that gave rise to a cost smaller than 500. The right panel shows the value of the cost. From this it is seen that only an appropriate linear combination of S_{in} and S_{dis} is well determined when only considering fetch limited growth. This is a well-known problem: the enhancement of wave growth by wind, can be counterbalanced by an appropriate increase of whitecap dissipation. Therefore the gradients with respect to S_{in} and S_{dis} are mirror-like, as can be seen from the right panel of Figure 2.

From the right panel of Figure 2, it is seen that the sensitivity of the cost to the bottom dissipation is very weak compared to the sensitivity to the wind input and whitecap dissipation. From the second iteration, the system lies in the shallow valley formed by J_{KC}. The value of J_{KC} is an order of magnitude smaller than its starting value (see Table 1). Therefore a change in S_{in} or S_{dis} will lead to a large deviation from this valley and therefore to strong gradients. J_{KC} does not depend on S_{bot}. Therefore the sensitivity of the shallow water cost to the different control parameters will be much more balanced. The agreement with the deep water situation

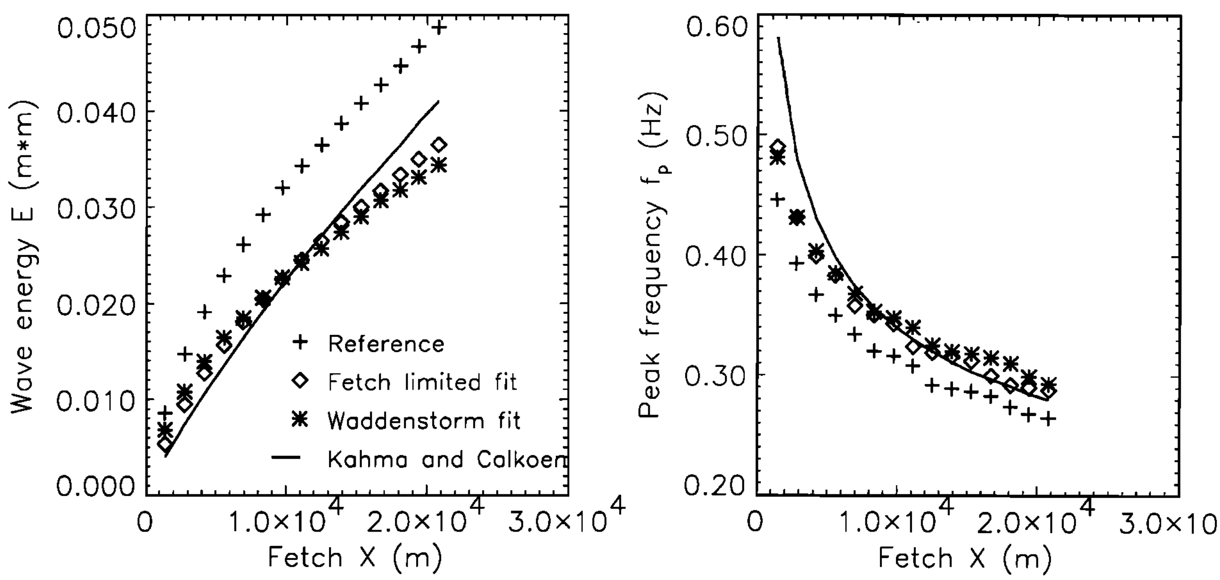

Figure 4. Comparison between WAM model results and the growth curves obtained by *Kahma and Calkoen* [1992] for the deep water fetch-limited case. The solid lines represent the growth curves, the pluses are WAM model results on the basis of its default setting, the diamonds represent the results from the optimal setting found from the fetch-limited growth run, while the asterisks are the outcome of the Wadden storm optimization.

can be seen as a kind of a strong constraint. It is mainly the shallow water part of the cost that is optimized from the fourth iteration. Therefore a change in C_{bot} will be significant, although the right panel of Figure 2 would suggest the opposite.

The absolute minimum of the valley corresponds to the third local minimum found by the minimization. It is also the most stable one. Its parameter setting is given in Table 1. From this it is seen that both the wind input term (21%) and the whitecap dissipation (37%) have been diminished considerably. The second considerable deviation from the default WAM setting is the increase of C_3, which concerns the relevance of the wave steepness in the whitecap dissipation.

Finally, the most profound change with respect to the default WAM setting is the strength of the bottom dissipation. The optimal value is 2.4 times as large as the JONSWAP value. Apparently, the muddy bed material is much more dissipative than the bed material near Silt, Germany, where the JONSWAP experiment [*Hasselmann et al.*, 1973] was performed.

The comparison between the WAM model results and data are given in Figure 4 and 5. In Figure 4 the deviation from the deep water Kahma and Calkoen growth curves for wave energy and peak frequency is shown. From this it is seen that the fit led to a considerable improvement of the agreement between WAM and these "data". In the left panel of Figure 5, the results for the central station (number 6) of Lake George are presented. The results for station 8 were comparable. For stations 1, 2, and 3 the agreement for the wave heights was equally good, but the peak frequencies were consistently overestimated ($\sim$ 0.1 Hz) by the optimized WAM model. Apparently, the freedom allowed in the control variable space, or the physics, were not sufficient to accommodate for this. No data were available for stations 4 and 7.

For the optimization run only a period of 12 hours was used. It was found, however, that the improvement remained for other periods. As an example, the results for June 12 are represented in the right panel of Figure 5. This period corresponds to a westerly wind with a strength between $U_{10} \sim 5$ - 15 m/s. So, although this represents a completely different situation, the optimized WAM model gives also a considerable improvement for this situation. Especially, the wave heights, which were too high for the default WAM setting, are reduced correctly by the improved bottom dissipation. The same is valid for station 8. For stations 1, 2 and 3, again the peak frequencies are too high, but the agreement for wave height is excellent.

It was found that the optimum found at the fourth iteration overestimated the period of June 12 considerably. This optimum suggests a reduction in S_{in} only. Although this will lead to splendid deep water results, it does not perform very well for Lake George in case of high wind speeds. Only a strong dissipative force, such as S_{bot} is capable of restricting the waves in a proper way.

3. Wadden Storm

The North Sea (see Figure 6) constitutes a suitable environment in which the combination of deep and shallow water and wind sea and swell can be studied. It

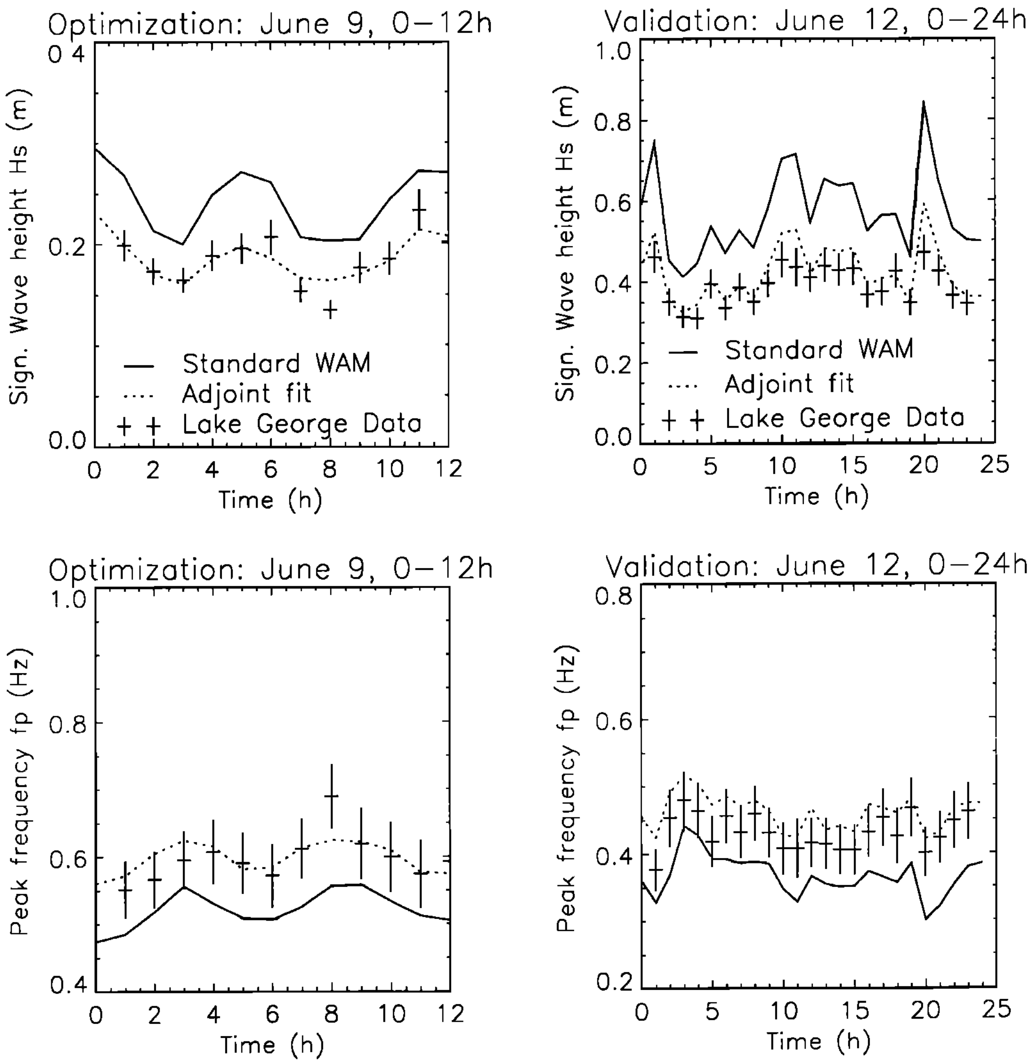

Figure 5. Comparison between WAM model results and Lake George data for station 6. The data obtained by *Young and Verhagen* [1996] are indicated by the error bars. The model results obtained from the default setting of WAM are in solid lines. The dotted lines represent the results on the basis of the adjoint fit. The optimization was performed for the period in the left panel. The right panel shows the consistency of the improvement.

contains a richer spectrum of wave phenomena than the situation studied in the previous section, in which only wind sea was present. Therefore it is expected that the observed wave fields in the North Sea will provide a more demanding constraint on the strength of the individual sources. Especially, it is expected that the absolute strengths of the wind input and whitecap dissipation can be better determined. This information will be hidden in swell components, in which the wind input source term is not effective. It contains the opportunity to separate the influence of S_{in} and S_{dis}. In addition, there is the availability of Wavec buoy data [*Kuik et al.*, 1988], which give directional information in addition to integrated parameters.

The Wadden storm (February 14-28, 1993) was selected as the test period. It contained a situation with extreme wave conditions. During the peak of the storm, significant wave heights up to 10 m were measured in the southern part of the North Sea. It will therefore constitute a severe test of the WAM physics. The Wadden storm was also selected as the test case for the ECAWOM project, a project funded by the European Committee, with as its goal the development of a fully coupled atmospheric-wave-ocean model, including a data assimilation setup. The work described in this paper was part of the ECAWOM project.

3.1. WAM Setup

At KNMI, the WAM model runs operationally for the North Sea. Its implementation, NEDWAM [*Burgers*, 1990; *Komen et al.* 1994], uses a grid running from 50.33° N to 72.33° N and from 7.00° W to 16.00° E. The grid spacing is 1/3 degree in the latitudinal direction

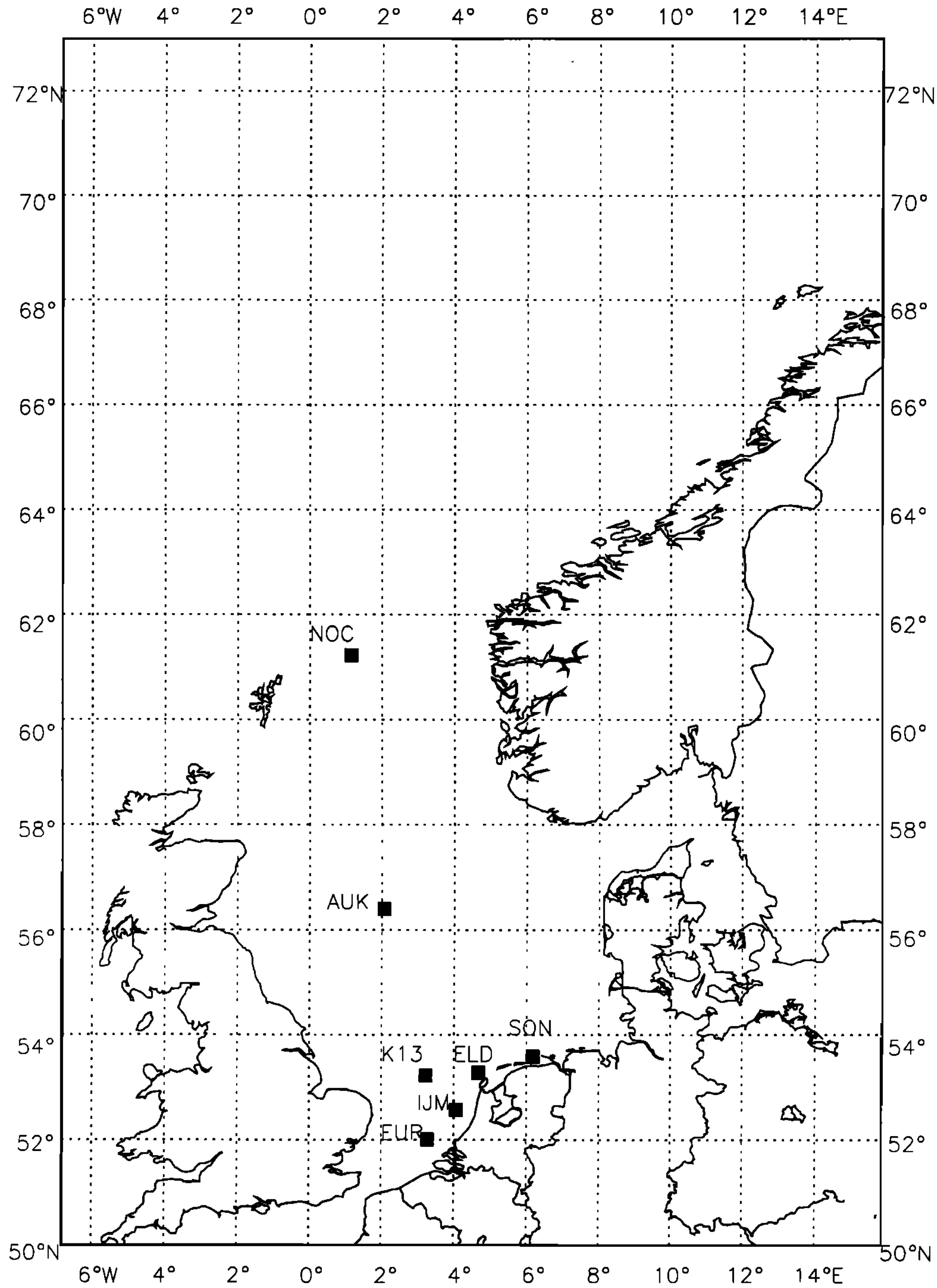

Figure 6. The location of the Wavec buoys in the North Sea. For the adjoint fit only the data obtained from the buoys AUK, K13, and EUR have been used. No data were available for NCO.

and 1/2 degree in the longitudinal direction. The minimum wave frequency used is 0.042 Hz, which corresponds to the default value of the global model running at the European Centre for Medium-Range Weather Forecasts. The model integration time step is 600 s.

The WAM model was driven with Limited-Area Model (LAM) winds rather than with High Resolution Limited-Area Model (HIRLAM) [*Kållberg,* 1990] winds, because in February 1997 the latter were not operational at KNMI, which had the consequence that the boundaries, which force the HIRLAM model, were not always correct. The resolution of the wind field was 2/3 degree in the latitudinal direction and 1 degree in the longitudinal direction.

In order to reduce the computational burden for the adjoint run, the resolution of the WAM grid was chosen to be equivalent to that of the driving wind field, so 2/3 degree in the latitudinal direction and 1 degree in the longitudinal direction. This therefore corresponds to a resolution that is twice as low as that of NEDWAM. Also the coverage of the grid region was chosen to be smaller than that of the NEDWAM grid. A grid running from 50.66° N to 66.00° N and from 7.00° W to 8.00° E was found to be appropriate. The minimum wave frequency was unaltered, the model integration time step used was 1800 s.

The results for this coarse resolution were tested against results obtained from finer resolutions for the Wadden storm period (February 14-28). No important deviations were found (~ 0.1 m in H_s).

3.2. Cost Function

The Wavec buoys are of the pitch-and-roll type, that is, they not only record time series of the surface elevation but also time series of the angles of the buoy in the x and y direction with respect to the horizontal plane. From these time series, six different cross correlations can be derived, which give information about the first five angular moments of the wave spectrum $F(f,\theta)$ as a function of frequency f. For details, see *Kuik et al.* [1988]. The Wavec data were extracted from the Contol Information Centre (CIC) database of the North Sea network, operated by Rijkswaterstaat in the Hydro Meteo Centre at Hook of Holland, Netherlands. This database contains records for six different buoys, AUK (56.4°N, 2.1°E), ELD (53.3°N, 4.7°E), EUR (52.0°N, 3.3°E), K13 (53.2°N, 3.2°E), SON (53.6°N, 6.2°E) and YM6 (52.6°N, 4.1°E), which are archived on a 3-hourly basis. Their locations are indicated in Figure 6.

In principle, the detailed information of the Wavec buoys could be used in the construction of the cost function. However, for such a detailed cost function, the model noise, described in section B3, appeared to scramble the local gradients too much. Therefore it was decided to compare only integrated parameters in the cost. We are fully aware of this unsatisfactory situation; however, as we will see, the results obtained from the adjoint fit were still satisfactory. Only the total wave energy, mean frequency, and mean direction of the Wavec data were compared to the WAM model results. To this end the following cost function was defined:

$$J(\vec{C}) = \sum_i 2N_i \left\{ \left(\frac{f_{\mathrm{mean},i} - f^d_{\mathrm{mean},i}}{f_{\mathrm{mean},i}} \right)^2 + \left(\frac{E_i - E_i^d}{E_i^d} \right)^2 + \left(\frac{\theta_{\mathrm{mean},i} - \theta^d_{\mathrm{mean},i}}{\pi} \right)^2 \right\}, \tag{15}$$

where N_i is the number of degrees of freedom used to convert the time series to energy spectra and the superscripts d denote the Wavec data.

In the cost function only the data obtained from AUK, K13, and EUR were used. The buoys near SON, ELD, and IJM are located rather close to the coast. Therefore the uncertainty in the local (shallow) water depth can modify the results considerably. In accordance with the previous section, the local water depth could be adjusted during the adjoint run. It was decided, however, to circumvent this complication by excluding the data obtained from these buoys from the adjoint run. It was found, as will be seen below, that the remaining data sets from AUK, K13 and EUR alone were able to give sufficient information.

3.3. Choice of the Control Variables

Because the North Sea embodies a situation in which more physical processes interact, more freedom in the model parameters was allowed. First of all, as in the previous section, the overall strength of S_{in} (i.e., β_m defined in (A4)), S_{dis}, and S_{bot} were allowed to vary, as well as the "steepness" parameter D_s (defined in (A5)). In addition, the strength of S_{nl} was taken as a control variable. A second parameter, besides β_m, that concerns the details of the wind input term is z_α (see (A3)). It was introduced by *Janssen* [1989, 1991] to account for gustiness of the driving wind field. Both a modification of β_m and z_α will affect the strength of S_{in}. The whitecap dissipation (A5) contains a parameter δ. It expresses the relative importance between the $k/<k>$ and $(k/<k>)^2$ term. This parameter was also allowed to be adjusted.

This leads to the following seven control variables:

$$\begin{aligned} \beta_m &\rightarrow C_1\beta_m \\ z_\alpha &\rightarrow C_2 z_\alpha \\ C_{nl} &\rightarrow C_3 C_{nl} \\ C_{\mathrm{dis}} &\rightarrow C_4 C_{\mathrm{dis}} \\ \delta &\rightarrow C_5\delta \\ D_s &\rightarrow C_6 D_s \\ C_{\mathrm{bot}} &\rightarrow C_7 C_{\mathrm{bot}}. \end{aligned} \tag{16}$$

3.4. Optimization

The WAM model was optimized for the 2-day period February 19-21. This is just before the maximum of the storm. In Figure 7 the evolution of the cost and the control variables is given. From Figure 7 it is seen that there is convergence to only one minimum and that this convergence is slower than for the fetch-limited growth case. The value of the cost decreases from an initial value of 128 to an optimal value of 66. The optimal values of the control variables are given in Table 2.

From the right panel of Figure 7 it appears that the mirror-like behavior between the strengths of wind input and whitecap dissipation is again evident. From this panel it is also seen that the sensitivity of the cost to the strength of the nonlinear interaction is small compared to the sensitivity to S_{in} and S_{dis}. In contrast to the fetch-limited case, where "spurious" dependencies were induced by the deep water cost acting as a strong

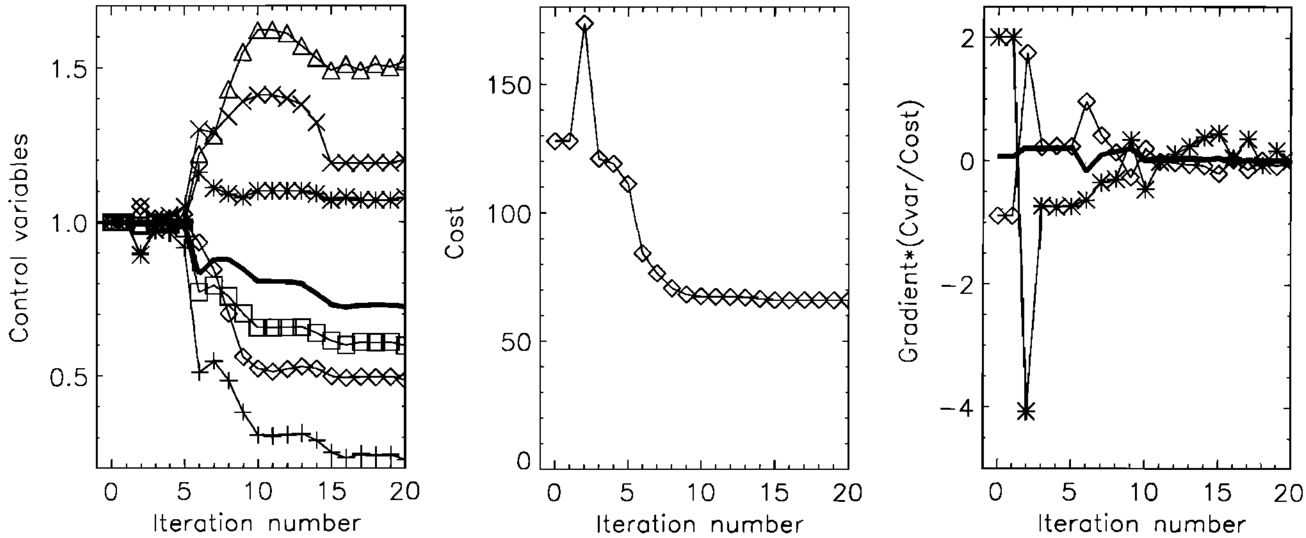

Figure 7. Optimization for the Wadden storm. (left) Evolution of the control parameters β_m (asterisks), z_α (pluses), C_{nl} (solid line), $C_{\rm dis}$ (diamonds), δ in $S_{\rm dis}$ (squares), $D_{\rm s}$ (triangles), and $C_{\rm bot}$ (crosses). (middle) Evolution of the cost. (right) Evolution of relative gradients for control variables β_m (asterisks), $C_{\rm dis}$ (diamonds), and C_{nl} (solid line).

constraint, this weak dependency is realistic. Although the presence of the nonlinear interaction is crucial (it provides the mechanism for redistributing wave energy), its precise form and strength appears to be less important. This observation supports the discrete interaction approximation: although it is only a very rough approximation to the exact nonlinear source term, it does give rise to correct wave spectra, because it shares the essential physical process of redistributing wave energy. Apparently, its precise form and strength is less important.

In Figure 8, scatterplots of the strength of the whitecapping versus β_m, z_α, and the cost is presented. Only points that gave rise to a cost lower than 70 are displayed. From this it is seen that the possible variation in the strength of the whitecapping is much more confined than in the fetch-limited case. The optimal ranges of the strength of $S_{\rm dis}$ between the two experiments overlap. Also the possible variation in the overall strength in $S_{\rm in}$ (defined by β_m) is quite small. However, the ranges of both runs do not overlap at all. In the fetch-limited growth situation a decrease of 21% is found, while the Wadden storm suggests an increase of 7%. The explanation for this mismatch is the variation in z_α, which was only allowed in the Wadden storm run. Although the possible variation is quite large (see the middle panel of Figure 8), it should be decreased by a factor of 3 or 4. The wave growth appears to be quite sensitive to a variation in this parameter. As can be seen from (A3), a decrease of z_α will lead to a decrease in wave growth. Therefore, effectively, the resulting fit does represent a suppression of the wind input term.

Table 2. Numerical Values of the Control Variables, Defined by (16), Before and After Optimization

Quantity	$C_{\rm var}$	Default	Fit	Final Value
β_m	C_1	1.0	1.07	β_m= 1.28
z_α	C_2	1.0	0.24	z_α= 0.0026
Strength S_{nl}	C_3	1.0	0.73	C_{nl}= 0.73
Strength $S_{\rm dis}$	C_4	1.0	0.50	$C_{\rm dis}$= 4.7×10^{-5}
δ in $S_{\rm dis}$	C_5	1.0	0.61	δ= 0.31
D_s in $S_{\rm dis}$	C_6	1.0	1.51	D_s= 3.0
Strength $S_{\rm bot}$	C_7	1.0	1.20	$C_{\rm bot}$= 0.0456
Cost function	J	128	66	

As was the case for the fetch-limited fit, the power D_s has been increased. The mixing parameter δ also has been decreased. Finally, it is found that the bottom dissipation should be increased somewhat.

The comparison between the WAM model runs and the Wavec data is displayed in Figure 9. From this it is seen that the wave heights for the default setting are already quite good but that the mean wave periods are too high. This deficiency is largely removed by the adjoint fit result. This can also be seen from the bottom panels of Figure 9, in which the quantity:

$$Y_m = \frac{H_s}{gT_m^2} \tag{17}$$

is plotted. In the previous section it was shown that the similar quantity Y_p (defined by (6)) was quite insensitive to wave age for the situation of wind sea. The same can be deduced for Y_m. For the present situation of mixed wind sea and swell, Y_m will be less constant, depending on the relative strength between the two. Still we believe that a misfit in this quantity mainly reflects model errors, rather than an error in the driving wind fields. It is therefore an appropriate tool to single

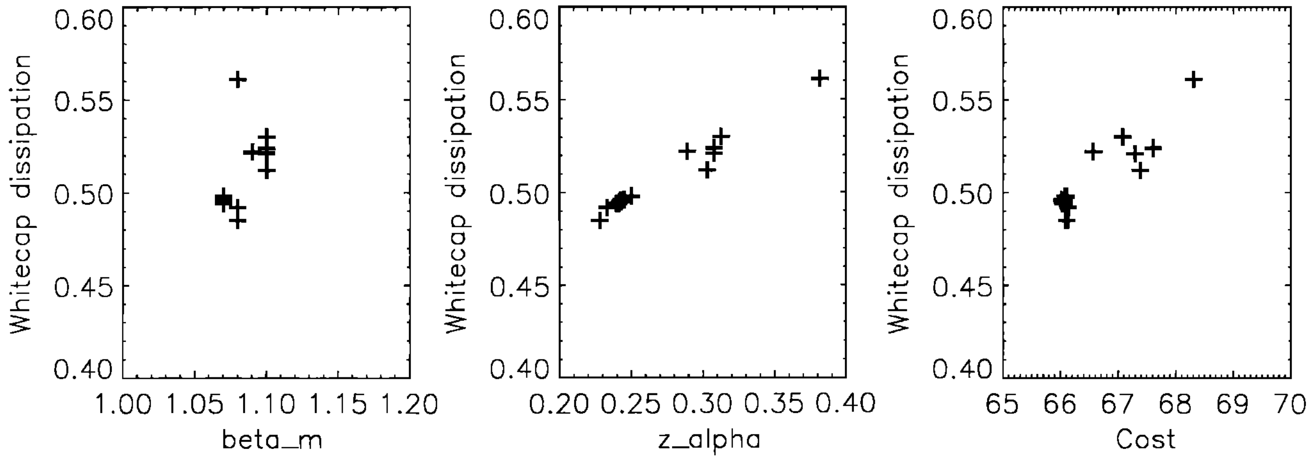

Figure 8. Scatterplot of the strength of the whitecapping versus the (left) absolute strength β_m of the wind input, (middle) the gustiness parameter z_α in the wind input, and (right) the cost. Only points explored by the adjoint optimization that gave rise to a cost lower than 70 are displayed.

out model errors. It is seen from the bottom panel of Figure 9 that indeed the consistent underprediction of Y_m has been removed.

In order to investigate the consistency of the adjoint fit, the optimized setting given in Table 2 was validated for the entire test series of the storm. Indeed, for the complete period, the wave heights were only mildly deflected, but the mean wave periods were improved consistently. As a result, the quantity Y_m was found to be reproduced much better. An example is given in Figure 10 where time series for EUR are given. From Figure 10 it is seen that the optimized parameter setting gives too low wave heights and too low wave period for the peak at February 19, 12 hours. The quantity Y_m, however, is very well represented. Therefore one might expect that the misfit at this date is due to an error in the wind field, because this will affect the wave height and mean period but will not affect Y_m.

As was already remarked, the overall picture of both adjoint fits is consistent: a combined suppression of the wind input and whitecapping and an increase of the power D_s in the whitecap source term. However, in detail, both fits differ. For the fit based on the fetch-limited case, the suppression of wind input was achieved by a decrease of β_m, while the fit based on the Wadden storm was accomplished by a decrease in z_α. Further, it was found that the minima found for both fits were relatively shallow, which gave rise to regions in control variable space that give results of comparable quality. Because the results obtained from the Wadden storm gave rise to the best defined minimum, it is expected that this fit should be preferred. In order to test this conjecture, the fetch-limited growth case was recalculated on the basis of the parameter setting found by the Wadden storm fit (see Table 2). Only for the strength of S_{bot} the value of $C_{\text{bot}} = 2.43 \times 0.038 = 0.092$ found by the fetch-limited fit was used, because this parameter depends very sensitively on the sediment. This led for the Lake George situation to time series that are almost identical to those obtained by the optimized run (parameters given in Table 1). The deep water growth curve for energy, however, appeared to be approximately 10% higher, the peak frequencies were almost unaltered. This result is presented in Figure 4. This difference is well within the uncertainty range of the deep water fetch-limited growth curves (2). Therefore we conclude that indeed the fit obtained by the Wadden storm (Table 2) gives also good results for the fetch-limited situation.

4. Conclusions

The adjoint of the full WAM model has been constructed with the aid of an automatic adjoint compiler. The resulting code, ADWAM, is efficient in computing time and in the storage required for the nonlinearities of the model. ADWAM can be used for many model options and for many types of control variables.

Due to the WAM model noise, the local gradient may be quite different from the more global behavior of the cost function. In such a case the usefulness of ADWAM is limited. Although it is not exactly clear when this problem arises, it was only found to be present when the cost singled out too much detail from the wave spectra. In order to ensure the usefulness of ADWAM in each situation, it is recommended that the locations of the WAM code that produce the model noise should be traced. If these locations cannot be replaced by smoother code, the adjoint at these locations should be derived by hand at the model equation level, rather than on the model code level.

As a first application of ADWAM, the model performance of WAM was improved by adjusting model parameters in the WAM source terms. Model results

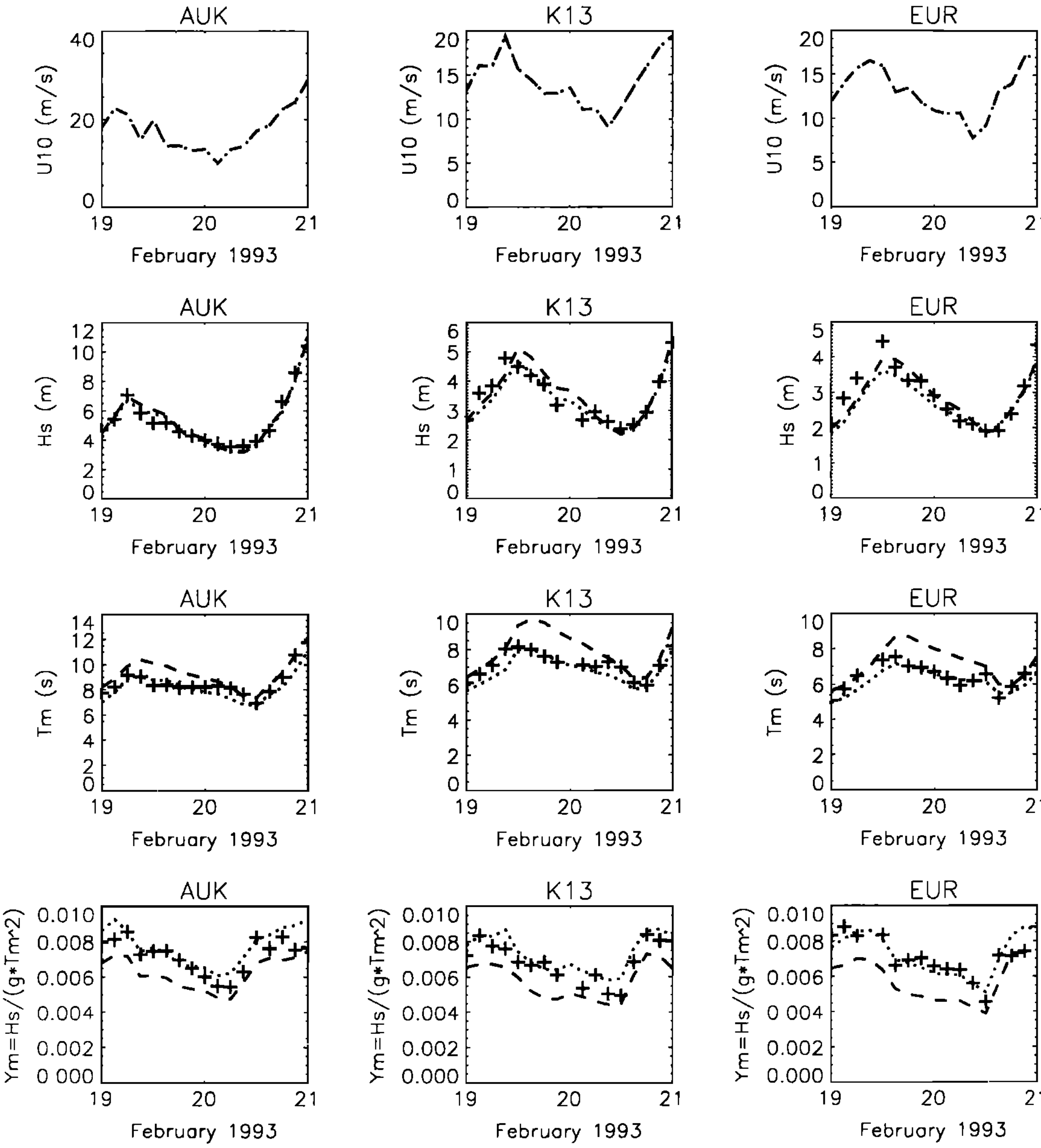

Figure 9. Comparison of significant wave height H_s, mean period T_m, and quantity Y_m, between WAM model results and the buoy's AUK, K13, and EUR for the optimization period February 19-21. The Wavec data are indicated by the pluses. The model results obtained from the default setting of WAM are represented by the dashed lines, while the results obtained from the optimal setting are given by the dotted lines. The top row shows the observed local wind speed U_{10}.

were compared to observations by the definition of a cost function. The optimal parameter setting was accomplished by minimizing the cost, using the MODULOPT minimization package developed by *Gilbert and Lemaréchal* [1989]. Gradients of the cost with respect to the model parameters were calculated by ADWAM.

For two physically quite different situations, adjoint optimizations were performed. The first situation considered fetch-limited growth. For this the WAM model was implemented on Lake George, using a very fine grid spacing (1.39 km). The second situation concerned a storm situation in the North Sea. Both adjoint fits led to the insight that wind input and whitecapping should be reduced and that the dependency of the wave steepness on the whitecapping should be increased. The combined reduction of wind input and whitecapping is in agreement with *Barzel* [1994]. It was found that the fetch-limited growth situation still left a considerable freedom in the absolute strength of the various sources. Only certain combinations of the sources, such as the combination between S_{in} and S_{dis} displayed in Figure 3, are well determined when one only considers wind sea. This conclusion was also drawn by *Barzel* [1994]. In his work it was recommended to use a more realistic situ-

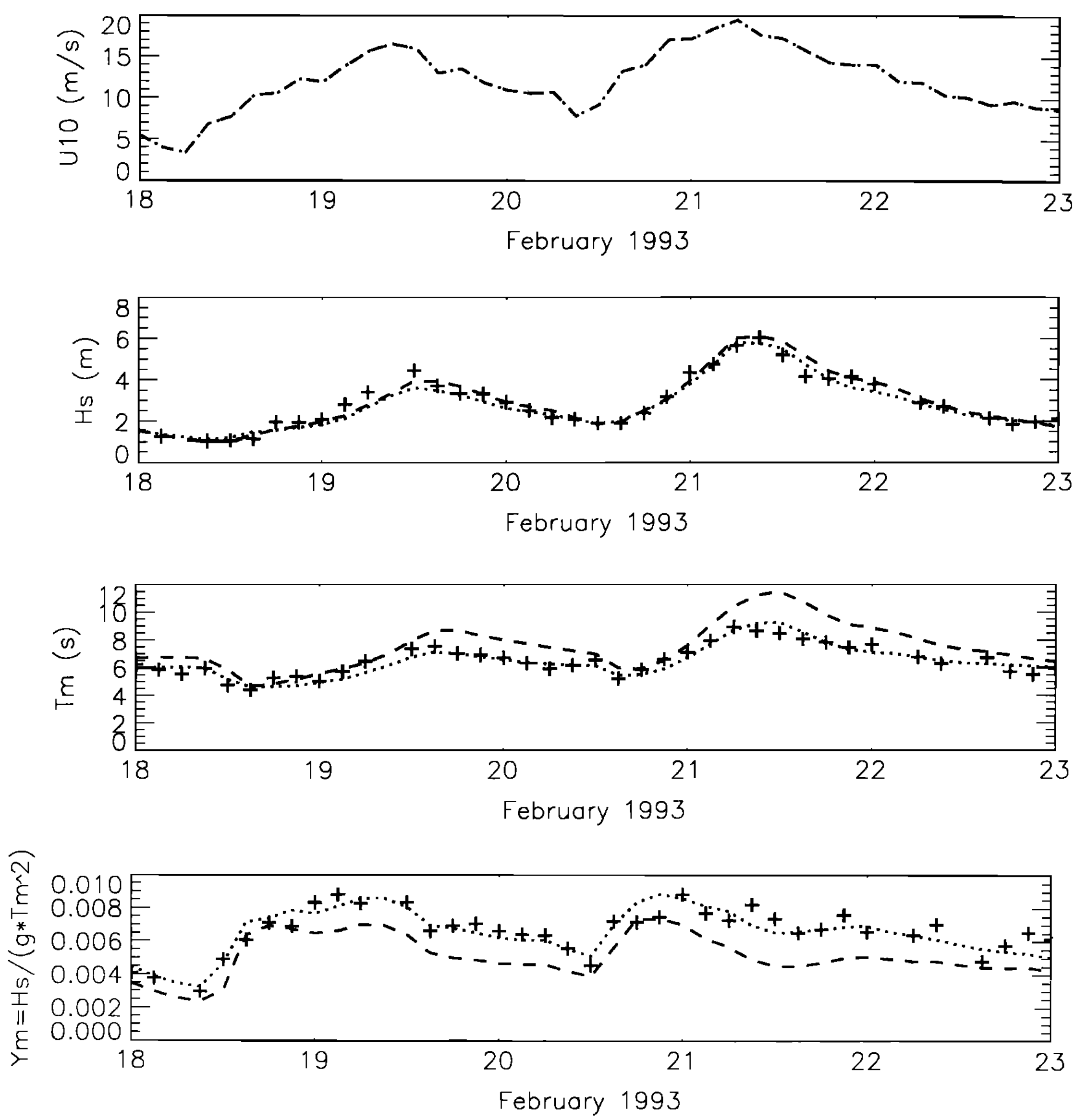

Figure 10. Validation of the optimized setting of the WAM model parameters for the EUR buoy for observed wind speed U_{10}, significant wave height H_s, mean period T_m, and quantity Y_m. The Wavec data are indicated by the pluses. The model results obtained from the default setting of WAM are represented by the dashed lines, while the results obtained from the optimal setting are given by the dotted lines. Only the period February 19-21 was used for the optimization.

ation, using the adjoint of the full dimensional WAM model. This is exactly what has been done in this paper. The fit obtained from the Wadden storm run at the North Sea left less freedom in the absolute values of the various parameters. This was expected, because it contains more complex wave situations. Its parameter setting, which is displayed in Table 2, gave a considerable improvement in model performance for all situations considered, that is. the North Sea, Lake George and for deep water fetch-limited growth. The difference between the involved scales and the wave fields between these situations is considerable. It would be very interesting to test whether this parameter setting (except for C_{bot}) would also lead to improved performance in other situations.

It was argued that the quantity $Y = H_s/(gT^2)$, $T = 1/f_p$ or $T = T_m$ is rather insensitive to the strength of the driving wind field. Therefore this quantity can be used as an indicator whether a misfit between model and data is due to model performance or to a bad quality in the driving wind fields. This information can be very useful, because not seldom (as was shown by *Cardone et al.* [1995]), the quality of model performance is masked by the error introduced by the uncertainty of the driving wind fields. In this light it is very interesting to note that all wind fields considered in the Surface Wave Dynamics Experiment (SWADE), discussed by *Cardone et al.* [1995], give rise to an underprediction of Y_p. This is consistent with what was observed at the Wadden storm. It must be induced by a model error.

Although the quantity $Y = H_s/(gT^2)$ can single out model errors, it would be highly desirable to adjust model parameters and wind fields simultaneously. The tool to accomplish this, ADWAM, exists. Therefore from a technical point of view this next step should be feasible.

Appendix A: Concise Description of the WAM physics

In this appendix an overview of the WAM physics is presented. A comprehensive description is given by *Komen et al.* [1994].

The WAM model describes the evolution of a two-dimensional (in frequency f and direction θ) ocean wave spectrum F:

$$\frac{dF}{dt} + \frac{\partial}{\partial\phi}\left(\dot{\phi}F\right) + \frac{\partial}{\partial\lambda}\left(\dot{\lambda}F\right) + \frac{\partial}{\partial\theta}\left(\dot{\theta}F\right) = S = S_{\text{in}} + S_{nl} + S_{\text{dis}} + S_{\text{bot}}, \tag{A1}$$

where (ϕ, λ) denotes latitude and longitude, and an overdot denotes a time derivative.

A1. Wind Input

The wind input and dissipation terms used in the latest version (cycle 4) of the WAM model are adopted from Janssen's quasi-linear theory of wind-wave generation [*Janssen*, 1989, 1991]:

$$S_{\text{in}} = \omega\frac{\rho_{\text{air}}}{\rho_{\text{water}}}\beta(x, z_0)x^2 F, \tag{A2}$$

z_0 is the roughness length,

$$x = \left(\frac{u_*}{c_p} + z_\alpha\right)\cos(\theta - \phi), \quad z_\alpha = 0.011 \tag{A3}$$

c_p is the phase speed, ω angular velocity, and $\theta - \phi$ is the angle between wave propagation and wind direction. The function $\beta(x, z_0)$ is given by

$$\beta = \frac{\beta_m}{\kappa^2}\mu \ln^4(\mu), \quad \mu = \frac{g z_0}{c_p^2}e^{\kappa/x} \leq 1, \tag{A4}$$

where $\beta_m = 1.2$ determines the overall strength of S_{in}, $\kappa = 0.41$ is von Kármán's constant, and g=9.81 m/s^2 is the gravitational acceleration.

A2. Whitecapping Dissipation

The dissipation source term is based on the whitecapping theory of *Hasselmann* [1974], with a modification made by *Janssen* [1989]. It is given by

$$S_{\text{dis}} = -C_{\text{dis}} < \omega > \left(\frac{\alpha}{\alpha_{\text{PM}}}\right)^{D_s}\left\{(1-\delta)\left(\frac{k}{< k >}\right) + \delta\left(\frac{k}{< k >}\right)^2\right\}, \tag{A5}$$

where

$$\alpha = E < k >^2 \tag{A6}$$

is the square of the average steepness of the spectrum and $\alpha_{\text{PM}} = 4.57 \times 10^{-3}$. Angle brackets indicate a relation to an average over the wave spectrum F. In WAM the values D_s=2, δ=0.5, and an overall strength $C_{\text{dis}} = 9.4 \times 10^{-5}$ are used.

A3. Nonlinear Interaction

In principle, the theory of surface waves is nonlinear. The lowest-order nonlinearities can be represented by *Hasselmann* [1968]:

$$S_{nl}(1) = C_{nl} \sum_{\text{quadruplets}} C(1,2,3,4)F(2)F(3)F(4). \tag{A7}$$

Here $C_{nl} = 1$ is a normalizing factor, and 1, 2, 3, and 4 denote the individual members of a wave quadruplet. The cross section $C(1,2,3,4)$ is only nonzero for resonating quadruplets:

$$\mathbf{k}_1 + \mathbf{k}_2 = \mathbf{k}_3 + \mathbf{k}_4, \quad \omega_1 + \omega_2 = \omega_3 + \omega_4. \tag{A8}$$

The integral over multiplets for the exact expression of S_{nl} is far too expensive for operational purposes. To overcome this problem, the so-called discrete interaction was proposed by *Hasselmann et al.* [1985] and *Hasselmann and Hasselmann* [1985]. This approximation assumes that only a small subset of quadruplets is given a nonzero cross section but such that the physical process is retained. This approach enabled the feasibility of third-generation wave models.

A4. Bottom Dissipation

In case of shallow water, wave energy will dissipate due to bottom friction:

$$S_{\text{bot}} = -2\frac{C_{\text{bot}}}{g}\frac{k}{\sinh(2kd)}F. \tag{A9}$$

Here k is the wave number and d is the local water depth. The normalizing factor C_{bot} depends on the nature and structure of the sediment. In WAM the value C_{bot}=0.038 (JONSWAP) is used.

A5. Limitation of Wave Growth

In the WAM model the source terms are integrated using a semi-implicit integration scheme. One ingredient of this integration scheme is that the wave growth per time step is limited to a certain fraction of a Pierson-Moskowitz spectrum. It was found by H. Hersbach and P.A.E.M. Janssen (Improvement of the short fetch behavior in the WAM model, submitted to *Journal of At-*

mospheric and Oceanic Technology, 1997) that the limitation used in cycle 4 of WAM is too restrictive in the case of very small grid spacings and time steps. As a result, WAM severely underpredicted wave heights when implemented on lakes. A good example of this is Lake George, which was used as one of the experimental setups in this paper. This shortcoming has been removed in a new version (cycle 5 [*Hersbach,* 1997]) of the WAM model. The results discussed in the present paper are all based on this corrected cycle.

Appendix B: Construction of ADWAM

B1. Use of the Adjoint Model Compiler AMC

In this appendix only a concise description of how the adjoint of WAM was constructed will be presented. A more detailed report is given by *Hersbach* [1997].

The adjoint of the full WAM (cycle 4) model has been constructed with the aid of an automatic adjoint code generator. This adjoint model compiler (AMC), which was developed by R. Giering of Max-Planck-Institut in Hamburg [*Giering and Kaminski,* 1997], simplifies the tedious work of development of adjoint code considerably. As input, AMC takes the Fortran 77 computer source code of the model under consideration, in this case WAM. As output, it returns a modified forward model source code and a Fortran 77 source code of the adjoint model, in this case ADWAM. The AMC is capable of detecting the nonlinearities within the forward model. These will then be stored (to file or memory) or, if possible, be recalculated. The bookkeeping of the storage of nonlinearities in the forward code and their restorage in the adjoint code is completely handled by the AMC. Because this bookkeeping can become quite complex, this is one of the strong points of AMC.

However, before AMC could be applied, some parts of the WAM source code had to be rewritten into a form that the AMC can handle and which leads to an optimal adjoint code, both in terms of calculation speed and required disk space. This was by far the most time-consuming part of the "adjoining operation". Details are given by *Hersbach* [1997].

B2. Performance and Applicability

The resulting adjoint code is efficient both in computing time and required disk space. ADWAM is about 70% slower than WAM itself. On the average, the computational burden of an adjoint model is proportional to the degree of the nonlinearity of the forward model. The calculation of the nonlinear interactions is the most time-consuming part of WAM. These are proportional to the wave spectrum cubed, and therefore the computation time of ADWAM is quite satisfactory.

Due to the semi-implicit integration scheme, the number of nonlinearities to be stored at each time step amounts to approximately the size of three restart spectra. The bulk of this amount is formed by the wave spectrum, the sum of the source terms and the functional derivative of this sum with respect to the wave spectrum. For realistic applications with many time steps and many grid points, this will result in a huge amount of required disk space. To avoid storage problems, the so-called check point method [*Griewank,* 1992] has been implemented. The idea is as follows. First one forward run is performed, at which at regular intervals restart spectra are stored (the check points). The first check point, C_1, is the initial spectrum, the last, C_n, is the final spectrum. No nonlinearities are stored. Next the model is rerun from C_{n-1} to C_n. This time nonlinearities are stored. The amount is $1/(n-1)$ times the amount for the whole trajectory from C_1 to C_n. Then the adjoint can be run from C_n to C_{n-1}, using these nonlinearities. Next the model is run from C_{n-2} to C_{n-1}. The device containing the previous nonlinearities is overwritten. The adjoint can then be run from C_{n-1} to C_{n-2}. This recipe is repeated until the adjoint has been integrated over the whole period C_n-C_1. In the optimal setting the number of check points is proportional to the square of the number of model time steps, nstep. The reduction of the amount of storage is enormous ($\sim \sqrt{\text{nstep}}$). The price is an extra forward model run. The extra computational burden (one forward run) is modest with respect to the total gradient computation time without check pointing ($\sim$ 1+1.7=2.7 forward runs).

ADWAM is the full adjoint of WAM. It can be used for arbitrary topography and bathymetry, grid spacing, time steps, spectral resolution, shallow and deep water runs, spherical or rectangular grids, with or without depth and/or current refraction. Parameters within the source functions can be taken as control variables. Also the driving wind fields and initial wave spectra can be used as control variables, which can be used for data assimilation purposes or sensitivity studies. In addition, the bathymetry can also be used as a set of control variables. ADWAM takes the dependencies of the local depth on S_{bot} and the shallow water corrections of S_{nl} into account. The depth dependency on the dispersion relation, however, is neglected by ADWAM. Therefore the computed gradient of the cost with respect to the bathymetry will not be completely correct, but this error is expected to be small.

The correctness of ADWAM was tested on the basis of a finite difference approximation to the gradient. For this, WAM was run for two different sets of control variables $\mathbf{c}$ and $\mathbf{c}+d\mathbf{c}$. When both sets are close enough, the difference in cost dJ can be approximated by $dJ = J(\mathbf{c}+d\mathbf{c}) - J(\mathbf{c}) = (\partial J/\partial \mathbf{c})\cdot d\mathbf{c} + \mathcal{O}(d\mathbf{c}^2)$. Starting with a $|d\mathbf{c}| = 1$ and reducing its magnitude, one expects that the fraction R between the linear adjoint difference and the finite difference will converge linearly to unity. This test was performed for several control variables and for all possible model options (shallow/deep water, spherical/rectangular grid, current and or depth refraction). Indeed all fractions converged linearly to unity.

B3. Model Noise

The construction of the adjoint at the computer source level has the advantage that one receives the exact adjoint to the computer model. Therefore it will calculate the exact local gradient of the cost function with respect to the control variables. However, a numerical model can contain many switches, such as IF statements. Therefore each set of control variables will give rise to its own passage of the model integration through these switches, as a result of which the cost function can become very rough and discontinuous. The size of the subspaces in control variable space which give rise to an identical switch passage is in general much smaller than the typical step size in a minimizing routine. When the cost function jumps too much, going from one region to another, the local adjoint gradient may not represent the desired more global behavior of the cost function very well.

The WAM model code contains many switches. Therefore one has to be very careful in using the adjoint. It was found that when a cost function was constructed which depends too much on the details of the wave spectrum, the numerical noise in the WAM model produced local gradients that can be totally different from the more global variations, that is, having wrong magnitudes and even wrong signs. Therefore one should as much as possible look at averaged model results. These averages can be averages over frequencies and direction, in which case one is only interested in integrated wave parameters. It can also be averages over a space and/or time domain of detailed wave information. Indeed, in the cases described in this paper, the use of averaged model results gave rise to local gradients that represented the global behavior of the cost in a sufficient way, that is, they could be successfully used by the optimization routine. It is not clear where and when the model noise starts to scramble the local behavior of the cost function. More research in this direction is desired.

Acknowledgments. This work was carried out as part of the European Coupled Atmosphere/Wave/Ocean-Model (ECAWOM) project, funded by the MAST (Marine Science and Technology) Programme of the European Union. We acknowledge comments and suggestions from Ralf Giering, Thomas Kaminski, Gerbrand Komen, Aart Voorrips, and Peter Janssen. We would like to thank Georg Barzel and Robert Long for their support at the initial stage of the project.

References

Barzel, G., Optimierung eines Seegangsmodells mit der adjungierten Methode, MPI Examsarbeit 26, 95 pp., Max-Planck-Inst. für Meteorol., Hamburg, August 1994.

Bauer, E., K. Hasselmann, I. R. Young, and S. Hasselmann, Assimilation of wave data into the wave model WAM using an impulse response function method, *J. Geophys. Res.*, *101* 3801-3816, 1996.

Burgers, G., A guide to the NEDWAM wave model, *Tech. Rep. WR-90-04*, 81 pp., R. Neth. Meteorol. Inst., De Bilt, Netherlands, 1990.

Cardone, V., H. C. Graber, R. E. Jensen, S. Hasselmann, and M. J. Caruso, In search of the true surface wind field in SWADE IOP-a: Ocean wave modelling perspective, *Global Atmos. Ocean Syst.*, *3*, 107-150, 1995.

Charnock, H., Wind stress on a water surface. *Q. J. R. Meteorol. Soc.*, *81*, 639-640, 1955.

De las Heras, M. M., and P. A. E. M. Janssen, Data assimilation with a nonlinear, coupled wind wave model, *J. Geophys. Res.*, *97*, 20261-20270, 1992.

De las Heras, M. M., G. J. H. Burgers, and P. A. E. M. Janssen, Variational data assimilation in a third generation wave model, *J. Atmos. Oceanic Technol.* *11*, 1350-1369, 1994.

De Valk, C. F., and C. J. Calkoen, Wave data assimilation in a third generation wave prediction model for the North Sea: An optimal control approach, *Tech. Rep. X38*, 123 pp, Delft Hydraul. Lab., Delft, Netherlands, 1989.

Donelan, M. A., Air-sea interaction, in *The sea, Vol. 9, Ocean Engineering Science*, edited by B. Le Méhauté and D. M. Hanes, pp. 239-292, John Wiley, New York, 1990.

Giering, R., and T. Kaminski, Recipes for Adjoint Code Construction, *ACM Trans. Math. Software*, in press, 1997.

Gilbert, J. Ch., and C. Lemaréchal, Some numerical experiments with variable-storage quasi-Newton algorithms, *Math. Programming*, *45*, 407-435, 1989.

Griewank, A., Achieving logarithmic growth of temporal and spatial complexity in reverse automatic differentiation, *Optim. Methods Software*, *1*, 35-54, 1992.

Hasselmann, K., Weak-interaction theory of ocean waves, *Basic Dev. Fluid Dyn.*, *2*, 117-182, 1968.

Hasselmann, K., On the spectral dissipation of ocean waves due to whitecapping, *Boundary Layer Meteorol.*, *6*, 107-127, 1974.

Hasselmann, K., et al., Measurements of wind-wave growth and swell decay during the Joint North Sea Wave Project (JONSWAP), *Dtsch. Hydrogr. Z.*, suppl. A, 8(12), 95 pp., 1973.

Hasselmann, S., and K. Hasselmann, Computations and parameterizations of the nonlinear energy transfer in a gravity-wave spectrum, 1; A new method for efficient computations of the exact nonlinear transfer integral, J. Phys. Oceanogr., *15*, 1369-1377, 1985.

Hasselmann, S., K. Hasselmann, J. H. Allender, and T. P. Barnett, Computations and parameterizations of the nonlinear energy transfer in a gravity wave spectrum, 2; Parameterizations of the nonlinear energy transfer for application in wave models, *J. Phys. Oceanogr.*, *15*, 1378-1391, 1985.

Hersbach, H., The adjoint of the WAM model, *Tech. Rep. KNMI-WR 97-01*, 28 pp., R. Neth. Meteorol. Inst., De Bilt, Netherlands, 1997.

Janssen, P. A. E. M., Wave-induced stress and the drag of air flow over sea waves, *J. Phys. Oceanogr.*, *19*, 745-754, 1989.

Janssen, P. A. E. M., Quasi-linear theory of wind wave generation applied to wave forecasting, *J. Phys. Oceanogr.*, *21*, 1631-1642, 1991.

Kahma, K. K., and C. J. Calkoen, Reconciling discrepancies in the observed growth of wind-generated waves, *J. Phys. Oceanogr.*, *22*, 1389-1405, 1992.

Kållberg, P. (ed.), The HIRLAM forecast model, level 1, documentation manual, Swedish Meteorol. and Hydrol. Inst., Norrköping, Sweden, 1990.

Komen, G.J., Cavaleri, M., Donelan, M., Hasselmann, K., Hasselmann, S., and P. A. E. M. Janssen, *Dynamics and Modelling of Ocean Waves*, 532 pp., Cambridge Univ. Press, New York, 1994.

Kuik, A. J., G. P. van Vledder, and L. H. Holthuijsen, A method for the routine analysis of pitch-and-roll buoy wave data, *J. Phys. Oceanogr.*, *18*, 1020-1034, 1988.

Monbaliu, J., Wind driven seas: Optimal parameter choice for the wind input term, *J. Wind Eng. Ind. Aerodyn.* *41-44*, 2499-2510, 1992a.

Monbaliu, J., Wind and waves. Investigation of an optimalization approach to parameter estimation. Ph.D. thesis, Dep. of Civ. Eng., Katholieke Univ. Leuven, Leuven, Belgium, 1992b.

Pierson, W. J., Jr., and L. Moskowitz, A proposed spectral form for fully developed wind seas based on the similarity theory of S. A. Kitaigorodskii, *J. Geophys. Res.*, *69*, 5181-5190, 1964.

Smith, S. D., et al., Sea surface wind stress and drag coefficients: The HEXOS results, *Boundary Layer Meteorol.*, *60*, 109-142, 1992.

Taylor, P. A., and R. J. Lee, Simple guidelines for estimating wind speed variations due to small-scale topographic features, *Climatol. Bull.*, *18*, 3-32, 1984.

Young, I., and L. A. Verhagen, The growth of fetch limited waves in water of finite depth, part I: total energy and peak frequency, *Coastal Eng.*, *29*, 47-78, 1996.

H. Hersbach, Royal Netherlands Meteorological Institute, P.O. Box 201, 3730 AE, De Bilt, Netherlands. (e-mail: hersbach@knmi.nl)

(Received January 27, 1997; revised September 12, 1997; accepted October 16, 1997.)